Cigarette smoke induction of S100A9 contributes to chronic obstructive pulmonary disease

Running heading: S100A9 contributes to COPD

Christopher Railwah[1], Alnardo Lora[1], Kanza Zahid[1], Hannah Goldenberg[1], Michael Campos[2], Anne Wyman[1], Bakr Jundi[1], Magdalena Ploszaj[1], Melissa Rivas[1], Abdoulaye Dabo[1,3], Susan M. Majka[4], Robert Foronjy[1,3], Mohamed El Gazzar[5], and Patrick Geraghty[1,3,*]

[1]Division of Pulmonary and Critical Care Medicine, Department of Medicine, State University of New York Downstate Health Sciences University, Brooklyn, NY, USA; [2]Division of Pulmonary, Allergy, Critical Care and Sleep Medicine, University of Miami Miller School of Medicine, Miami, Florida, USA; [3]Department of Cell Biology, State University of New York Downstate Health Sciences University, Brooklyn, NY, USA; [4]Department of Medicine, Division of Pulmonary, Critical Care and Sleep Medicine, National Jewish Health, Denver, CO, USA; [5]Department of Internal Medicine, East Tennessee State University College of Medicine, Johnson City, TN, USA.

*Corresponding author: Patrick Geraghty, Ph.D., Division of Pulmonary and Critical Care Medicine, SUNY Downstate Health Sciences University, 450 Clarkson Ave, Brooklyn, NY 11203, USA; Telephone: (718) 270-3141; Fax: (718) 270-4636; E-mail: Patrick.Geraghty@downstate.edu

Author Contributions. Performed the experiments: CR, AL, KZ, HG, BJ, MP, MR, AD, and PG. Analyzed the data: CR, AL, SM, ME, and PG. Contributed reagents/materials/analysis tools: RF, MC, AW, ME and PG. Conceived study: PG. Designed the experiments and wrote the paper: CR and PG. All authors assisted in the editing of the manuscript.

Abstract

S100 calcium-binding protein A9 (S100A9), is elevated in plasma and bronchoalveolar lavage fluid (BALF) of COPD patients and aging enhances S100A9 expression in several tissues. Currently, the direct impact of S100A9-mediated signaling on lung function and within the aging lung is unknown. Here, we observed that elevated S100A9 levels in human BALF correlated with age. Elevated lung levels of S100A9 were higher in older mice compared to young animals and coincided with pulmonary function changes. Both acute and chronic exposure to cigarette smoke enhanced S100A9 levels in age-matched mice. To examine the direct role of S100A9 on the development of COPD, *S100a9*$^{-/-}$ mice or inhibited activity with paquinimod, and exposed the models to chronic cigarette smoke S100A9 depletion and inhibition attenuated loss of lung function, pressure-volume loops, airway inflammation, lung compliance, and $FEV_{0.05}$/FVC, compared to age-matched wild type or vehicle administered animals. Loss of *S100a9* signaling reduced cigarette smoke-induced airspace enlargement, alveolar remodeling, lung destruction, ERK and c-RAF phosphorylation, MMP-3, MMP-9, MCP-1, IL-6, and KC release into the airways. Paquinimod administered to non-smoked aged animals reduced age-associated loss of lung function. Since fibroblasts play a major role in the production and maintenance of extracellular matrix in emphysema, primary lung fibroblasts were treated with the ERK inhibitor, LY3214996, or the c-RAF inhibitor, GW5074, resulting in less S100A9-induced MMP-3, MMP-9, MCP-1, IL-6, and IL-8. Silencing TLR4, RAGE or EMMPRIN prevented S100A9-induced phosphorylation of ERK and c-RAF. Our

data suggest that S100A9 signaling contributes to the progression of smoke and age-related COPD.

Keywords: Cigarette smoke, S100A9, kinase, pulmonary function, aging

List of abbreviations

S100 calcium-binding protein A9, S100A9; chronic obstructive pulmonary disease, COPD; damage-associated molecular patterns, DAMPs; respiratory syncytial virus, RSV; forced expiratory volume, FEV; forced vital capacity, FVC; pressure -volume, PV; Bronchoalveolar lavage fluid, BALF; lactate dehydrogenase, LDH; phosphate buffer saline, PBS; bovine serum albumin, BSA; Room air, RA; matrix metalloprotease, MMP; Institutes of Health and Institutional Animal Care and Use Committee, IACUC; protein tyrosine phosphatase 1B, PTP1B; vitamin D receptor, VDR; human bronchial epithelial, HBE; nitric oxide, NO; E26 transformation-specific, ETS; toll-like receptor 4, TLR4; advanced glycosylation end product-specific receptor, AGER; Basigin, BSG

Introduction

Chronic obstructive pulmonary disease (COPD)is the fourth leading cause of death in the US. The CDC attributes over 480,000 deaths annually or about 1 in 5 deaths to cigarette smoke (61). Exposure to cigarette smoke is the primary environmental factor associated with the development of COPD in the developed

world. Cellular responses triggered by cigarette smoke cause the release of inflammatory and proteolytic mediators that contribute to the pathogenesis of COPD (21). There are several proposed mechanisms that lead to loss of lung function, including chronic inflammation (10), accumulation of secretions, protease responses (25), matrix remodeling, apoptosis (48), immunosenescence (43), and damage to airway mucosa (4). Importantly, COPD is regarded as an age-related disease, with the incidence rate rising with increasing age (78). During the normal aging process, pulmonary function begins to decline as a consequence of structural and physiological changes to the lung (44). There is also a strong association between smoke-induced diseases and damage-associated molecular patterns (DAMPs) (24, 49). DAMPs are endogenous molecules released from damaged or dying cells and activate the innate immune system via pattern recognition receptors. Despite having important roles in immune responses, several DAMPs are associated with disease pathogenesis, including S100 calcium-binding protein A9 (S100A9) (24). However, apart from elevated levels of S100A9 observed in the serum of COPD patients during an exacerbation (50) and in the BALF of exacerbation-free COPD patients (24) and S100A9 expression in many tissues enhances with age (68), we currently know little about its functional role in disease progression and the aging lung.

There are additional studies linking S100A9 to other pulmonary and cardiovascular diseases, with plasma S100A8/A9 levels associated with pediatric obstructive sleep apnea and may reflect an increased risk for cardiovascular morbidity (37). S100A9 frequently forms a heterodimer with S100A8 and both play an important role in many biological processes (74) but S100A8 and S100A9

are not always co-expressed (40). S100A9 is expressed at low levels in healthy tissue but is frequently observed in diseased tissue (20), and infiltrating immune cells (6). Intracellularly, S100A9 is known to regulate NADPH oxidase activity (6), which is a major source of reactive oxygen species in neutrophils. Extracellularly, high concentrations of S100A9 are observed at tissues with elevated inflammation or in the serum of patients with inflammatory diseases (13). In cardiovascular disease, plasma S100A9 levels correlate with blood neutrophils counts and with the incidence of coronary events and cardiovascular mortality (14). Our group determined that enhanced S100A9 signaling coincides with lung damage during respiratory syncytial virus (RSV) infection in mice (24). We have also determined that S100A9 is enhanced by cigarette smoke exposure and further enhanced during viral exacerbations in mice and human primary lung cells (24).

S100A9 is highly expressed in phagocytes, is elevated in COPD samples, and triggers degranulation of neutrophils releasing inflammatory and proteolytic enzymes (64). Therefore, we tested the hypothesis that S100A9 signaling in the lung contributes to age related changes in pulmonary function as well the development of COPD. We utilized animals genetically deficient for *S100a9* and paquinimod, a chemical inhibitor of S100A9 to explore the impact of *S100a9* deficiency or inhibition on lung structure and function and signaling changes during chronic smoke exposure and in aged animals. We utilized BALF and human primary lung fibroblasts to correlate S100A9 levels to age and to allow modulation of S100A9 responses *in vitro*, respectively. Fibroblast were utilized as they expressed S100A9-mediated cytokines and proteases and fibroblasts play a

major role in the production and maintenance of extracellular matrix in emphysema (45, 69). DAMP-associated receptors, kinases, cytokines, and proteases were investigated in lung fibroblasts to further elucidate molecular mechanisms regulated by S100A9 in COPD.

Methods

Human Samples

BALF was collected from healthy never smokers, smokers, and COPD patients free from exacerbations for 6-months (see Table 1 for demographics). Written informed consent was obtained from all study participants and was approved by the Institutional Review Board of the University of Miami and conformed to the Declaration of Helsinki.

Animal models

S100a9$^{-/-}$ mice (3), on a C57BL/6J background, were maintained in a specific pathogen-free facility at SUNY Downstate Medical Center. We chose to investigate the *S100a9*$^{-/-}$ as lung levels of *S100a9* were similar in wild type and heterozygous animals (Supplemental Fig. S1 (https://figshare.com/s/c1ff26d650bb24d1e954)). Both male and female mice, 8-week-old, were used at the initiation point for the majority of experiments. Mice were whole-body exposed to cigarette smoke in a chamber (Teague Enterprises, Davis, CA, USA) for three hours a day, five days per week at a total particulate matter concentration of 80-120 mg/m^3. Smoke exposure was continued for 6 months. Marlboro cigarettes were used to generate cigarette smoke. A/J mice

were used for the paquinimod studies. Oral paquinimod (Active Biotech AB, Sweden) was daily administered to animals at a final concentration of 3.75 mg/kg. Paquinimod is water-soluble, and control animals received water only as a vehicle. Mice received paquinimod (1) throughout the smoke study, or (2) 2-months into a 4-month smoking study, or (3) daily for 2 months in aged animals without smoke exposure. A cohort of C57BL/6J animals were aged (18-months) to compare age-dependent changes in S100A9 levels and the impact of paquinimod on lung function. Equally, age-matched animals were exposed to acute (1-month) or chronic smoke (6-months) exposure. All animal experiments were performed with approval from SUNY Downstate Health Sciences University's Institutional Animal Care and Use Committee. This study was performed in strict accordance with the recommendations in the Guide for the Care and Use of Laboratory Animals of the National Institutes of Health and Institutional Animal Care and Use Committee (IACUC) guidelines.

Expiratory measurements

Mice were anesthetized with an intraperitoneal (ip) injection of ketamine/xylazine hydrochloride solution (100/10 mg/kg; Millipore Sigma, Burlington, MA, USA). Animals were tracheostomized and connected via an endotracheal cannula to the SCIREQ flexiVent system (SCIREQ Inc., Montreal, Canada). After initiating mechanical ventilation, animals were paralyzed with 1 mg/kg pancuronium bromide (Millipore Sigma) via ip injection and several pulmonary function measurements (pressure-volume (PV) loops, lung compliance, compliance, and forced expiration extension (FEV) in the first 0.05 seconds of forced vital capacity

(FVC)) performed, as previously described (62). The area under the curve (AUC) of the PV loops was calculated for each animal.

Histology and lung immune cell measurements

Following euthanasia by cervical dislocation, the lungs underwent pressure-fixation and morphometric analysis in accordance with our previously published protocol (23) and in accordance with the ATS/ERS issue statement on quantitative assessment of lung structure (35). Fixed step sections (4-μm in thickness) every 200 μm of paraffin-embedded lungs were H&E stained. The lung was imaged with high-throughput scanner, Leica AT2. Whole slide scans of several layers were cropped into multiple images (at least 40 images per animal) before performing histology analysis based on stereological principles. Mean linear intercept analysis was performed as previously described (22). Alveolar boundary size and ductal destructive measurements were performed on images of the H&E stained tissues, as previously described (77). Bronchoalveolar lavage fluid (BALF) and BALF cells were obtained from animals of each group. BALF cells were cyto-centrifuged onto slides to determine macrophage and neutrophil numbers. Cells were stained with Diff-Quik stain and at least 200 cells were examined per slide. Goat polyclonal anti-S100A9 antibody (Santa Cruz Biotechnologies) was utilized to stain sections for immunohistochemistry. Briefly, deparaffinized sections underwent antigen retrieval using tri-sodium citrate at pH 6 for 30 minutes in a 98 ^{o}C water bath. After allowing the sections to cool, they were washed in PBS containing 0.05% Tween 20 (PBST) and blocked in 3% bovine serum albumin (BSA) in PBS for 1 hour at room temperature. Goat polyclonal anti-S100A9 antibody (Santa Cruz Biotechnologies) was added in 3%

BSA and incubated overnight at 4 ^{o}C on a rocking shaker. Sections were washed in PBS with tween 3 times for 10 minutes. Detection was by an avidin-biotin complex (ABC)–based method (Vector Laboratories, Burlingame, CA) using a biotinylated secondary antibody, which is linked to an ABC-enzyme complex, horseradish peroxidase. 3,3′ Diaminibenzidine (Vector Laboratories) was used as a substrate for peroxidase complexes yielding a brown reaction product at the site of the target antigen. Sections were counterstained with hematoxylin (blue). Isotype control goat IgG was used as a negative control.

BALF analysis

Mouse and human MMPs, cytokines, and S100 (A8 and A9) proteins were examined in BAL fluid using beads assays (MILLIPLEX MAP MMP Magnetic Bead and MILLIPLEX Cytokine Magnetic Bead Panels, Millipore Sigma, Billerica, MA, USA; R&D Systems Magnetic Luminex Assays) with the Bio-Rad Bio-Plex 200 system. Mouse desmosine levels were measured in concentrated BALF using the Biorbyt Mouse Desmosine ELISA Kit, as recommended by manufacturers (Cat # orb409382, Biorbyt LLC, San Francisco, CA, USA). Human BALF data were standardized to total urea concentrations, as determined by a commercially available assay per manufacturers' instructions (Abnova, Walnut, CA, USA).

Western blot and RT-PCR

Protein was collected from lung tissue by bead beater disruption (Minibeadbeater-16, BioSpec Products, Bartlesville, OK, USA). Tissue was

placed in radioimmunoprecipitation assay buffer with 50mg of 1 mm diameter Zirconia beads (BioSpec Products) and disrupted for 30 seconds in the bead beater. Fibroblasts were also lysed with the same buffer. Soluble proteins were collected following 10-minute centrifugation at 13,000 x g at 4°C. Immunoblots for ERK phosphorylation (Thr202/Tyr204 and total ERK1/2), c-RAF phosphorylation (Ser259 and total c-RAF), β-Actin and GAPDH (all antibodies from Cell Signaling Technologies, Beverly, MA, USA) were performed to confirm equal levels of protein were loaded per sample. Chemiluminescence detection was performed using the Bio-Rad Laboratories Molecular Imager ChemiDoc XRS+ imaging system. Densitometry was performed and represented as a ratio of pixel intensity of the phosphorylated ERK or c-RAF compared to total ERK or c-RAF, using Bio-Rad Laboratories Image Lab software (version 4.0, build 16). This densitometry ratio was defined as densitometry units (DU).

Gene expression was determined by qPCR using Taqman probes (Life Technologies/Applied Biosystems, Carlsbad, CA, USA). RNA was isolated using the Qiagen RNeasy kit following tissue or cell homogenization and mRNA was reverse transcribed using the Applied Biosystems high capacity cDNA kit (Life Technologies). qPCR was performed on the Bio-Rad CFX384 real-time system. All qPCR results are represented as relative quantification (RQ) compared to room air or nonsmoker controls and corrected to *ACTB* and *GAPDH* levels, using the ΔΔCt method.

Cell cultures

Primary adult pulmonary fibroblasts expanded in cell culture from the lung tissues of healthy controls were purchased from PromoCell (Heidelberg, Germany). Fibroblasts were cultured in DMEM (Corning Cellgro, Manassas, VA) supplemented with 10% bovine calf serum (BCS; HyClone Laboratories, GE Healthcare Life Sciences, Logan, UT), 2 mM l-glutamine (Gemini Bio-Products, West Sacramento, CA), 1 mM sodium pyruvate, MEM nonessential amino acids solution, and antibiotic-antimycotic (10,000 units/ml penicillin, 10,000 μg/ml streptomycin, and 25 μg/ml amphotericin B), all from GIBCO Life Technologies (Thermo Fisher Scientific, Waltham, MA). Fibroblast cultures were maintained in T75 culture flasks (Nest Biotechnology, Rahway, NJ) in a humidified atmosphere with 5% CO_2 at 37°C. For experiments, fibroblast cultures were incubated with DMEM medium containing the same supplements and 0.5% BCS for at least 12 hours before testing. Fibroblasts were passaged by washing with filtered PBS, trypsinizing with 2–5 ml 0.25% trypsin-EDTA (GIBCO Life Technologies), and reconstituting cells in DMEM with 10% BCS before transfer to new T75 flasks, dishes, or six-well plates. In all experiments, fibroblast cell cultures were tested in passages four to seven. The ERK inhibitor, LY3214996, or the c-RAF inhibitor, GW5074 (both purchased from Selleckchem.com, Houston, TX, USA) were added to the media of the cultures and incubated for 24 hours at 37 °C, 5% CO_2. Cells were also transfected with siRNA specific for TLR4, AGER, BSG and scrambled control (QIAGEN) prior to treatment with recombinant human 1 μg/ml S100A9 protein (Novus Biologicals, Centennial, CO). Cells were collected for protein or RNA analysis.

Statistical analyses

The majority of the data are expressed as dot plots with the means ± S.E.M highlighted. Normality testing (D'Agostino & Pearson omnibus normality test) was performed on all data sets. A comparison of groups was performed by Student's t-test (two-tailed) when data passed the normality test and by Mann Whitney test if data did not pass normality testing. Experiments with more than 2 groups were analyzed by 2-way ANOVA with Bonferroni posttests analysis. p values for significance were set at 0.05 and all significant changes were noted with the exact p value. All analyses were performed using GraphPad Prism Software (Version 6.0h for Mac OS X).

Results

Age and cigarette smoke exposure enhances lung S100A9 levels. Previously, we demonstrated that S100A9 levels are elevated in COPD BALF samples (24). Here, we investigated whether age, smoking and disease status correlate with lung S100A9 levels. Within the subject cohort, S100A9 levels were significantly elevated in COPD subjects compared to nonsmoker controls (Fig. 1A). S100A9 concentration within BALF from nonsmokers (R^2=0.53 and P=0.011), smokers (R^2=0.19 and P=0.020), and COPD (R^2=0.17 and P<0.001) subjects correlated with age (Fig. 1B). As a binding partner and signaling modulator of S100A9, S100A8 levels were measured in the same cohort. However, no significant changes in BALF S100A8 levels were observed (Supplemental Fig. S2A-B (https://figshare.com/s/32b82a1f167002ff343b)).

In order to understand the role for S100A9 during the processes of aging and the development of COPD, we analyzed murine models to confirm our

results in the patient cohort. As the development of chronic lung diseases are associated with aging, we examined gene expression and BALF levels of S100A9 in young (7-weeks old) and old (18-months old) C57BL/6J (Fig. 2A) mice. Older mice expressed and secreted higher levels of S100A9 than young mice (Fig. 2A). This was also true for S100A8 (Supplemental Fig. S2B-C (https://figshare.com/s/32b82a1f167002ff343b)). To examine whether *S100a9* expression correlated with age-mediated changes in lung function and morphometry, we analyzed pressure volume loops, lung compliance, $FEV_{0.05}$/FVC, and mean linear intercept (MLI) in the same young and old mice. Aged mice showed changes in both physiology and histology parameters consistent with the development of emphysema (Fig. 2B). Equally, elevated IL-6 and KC were observed in the BALF of aged animals (Fig. 2C).

Next, we sought to determine whether cigarette smoke exposure affected the expression of S100A9. Age-matched mice were exposed to room air, 1 (acute) or 6 (chronic) months of cigarette smoke and analyzed at 8-months of age (Fig. 2D). Both acute and chronic exposure to cigarette smoke enhanced S100A9 expression and secretion in C57BL/6J mice (Fig. 2D). BALF S100A8 was also increased (Supplemental Fig. S2C-D (https://figshare.com/s/32b82a1f167002ff343b)). Immunohistochemistry demonstrated that S100A9 is localized to infiltrating immune cells as well as airway epithelial cells (Fig. 2E). We also identified that airway epithelium and immune cells are a source of S100A9. Therefore, both age and smoke exposure influence S100A9 levels in the murine models, recapitulating our patient cohort data.

***S100a9* deficiency reduces cigarette smoke-induced loss of lung function.** Since increased levels of S100A9 expression and release into the BALF were correlated to loss of lung function, the significance of S100A9 signaling was assessed by genetic knock-out. We used the Scireq flexivent system to determine pulmonary function in wild type and *S100a9*$^{-/-}$ mice following room air or 6 months exposure to cigarette smoke. Knockout of S100A9 was confirmed by analysis of lung and BALF (Supplemental Fig. S1 (https://figshare.com/s/c1ff26d650bb24d1e954)). As expected, chronic smoke exposure altered lung compliance, $FEV_{0.05}$/FVC, and pressure-volume loops in wild type animals (Fig. 3A-B). However, *S100a9* deficient animals were less susceptible to functional changes as a result of smoke exposure (Fig. 3A-B). Similarly, analysis of histology demonstrated that *S100a9* deficiency significantly attenuated airspace enlargements, the number of alveolar airspaces and ductal/destructive fraction compared to wild type smoke-exposed animals (Fig. 3C-D). This data demonstrates that S100A9 contributes to structural and physiological changes to the lung.

***S100a9* deficient animals have reduced immune cell infiltration and associated cytokine and protease signaling following smoke exposure.** Inhibition of S100A9, in an arthritis animal model, preserved the structural integrity of bone and collagen and reduced inflammation (11). Therefore, we examined the impact of S100A9 on inflammation and protease production in *S100a9*$^{-/-}$ mice. *S100a9* deficiency reduced cigarette smoke-induced immune cell infiltration (Fig. 4A), and MCP-1, IL-6, and KC secretion into the airways (Fig. 4B). No S100A9-mediated changes were observed for IL-5, IL-9, IL-13, IL-17,

and Eotaxin (Supplemental Fig. S3A (https://figshare.com/s/6e206effdb27b4690bd0)). In human osteoarthritis synovium, the S100A9 inhibitor paquinimod blocks MMP-1 and MMP-3 secretion (58), which could impact on COPD (15). Therefore, we examined the expression of several MMPs in all animal groups. Loss of *S100a9* expression resulted in reduced MMP-3 and MMP-9 in the BALF of smoke-exposed mice (Fig. 4C). No S100A9-mediated changes were observed for MMP-2, MMP-8, and MMP-12 (Supplemental Fig. S3B (https://figshare.com/s/6e206effdb27b4690bd0)). Smoke-exposed *S100a9*$^{-/-}$ mice had reduced desmosine in their BALF compared to wild type mice (Fig. 4C), suggesting less elastin degradation within the lungs. We evaluated possible pathways that could be responsible for these S100A9-mediated signaling downstream effects and determined that loss of S100A9 influenced ERK and c-RAF phosphorylation (Fig. 4D). No S100A9-mediated changes were observed for Src, JNK, and p38 (Supplemental Fig. S4 (https://figshare.com/s/ac481e9a2b58d580526d)). Therefore, S100A9 mediates several cytokines, proteases, and kinases during smoke exposure possibly via ERK and c-RAF.

Early administration of paquinimod prevents smoke-induced COPD in mice. To determine whether the S100A9 inhibitor, paquinimod, could prevent the loss of lung function observed in COPD subjects, we performed a series of exposure studies in mice. First, to determine whether long-term administration of paquinimod exhibited any notable toxicity, animal weight and liver to body weight ratios were determined in mice receiving daily doses of paquinimod for 2 months.

No significant changes in animal weight or liver to body weight ratios were observed (Fig. 5A). Since long term paquinimod treatment had little to no negative effects in mice, paquinimod was first administered to mice at the same time as smoke exposure. This approach determined whether extracellular S100A9 was contributing to lung disease initiation. Similar to *S100a9* deficiency, treatment with paquinimod prevented loss of lung function in wild type mice determined by Flexivent measurements of $FEV_{0.05}$/FVC, lung compliance and pressure-volume loops (Fig. 5B-C). Equally, when quantifying histology changes to lung tissue, paquinimod reduced smoke-induced airspace enlargement, alveolar remodeling, and destruction (Fig. 5D-E). Early administration of paquinimod also reduced smoke-induced inflammation in the airways (Fig. 6A), the release of MCP-1, IL-6, KC (Fig. 6B), MMP-3, MMP-9 and desmosine into the airways (Fig. 6C). Paquinimod also prevented phosphorylation of ERK and c-RAF (Fig. 6D). Similar to *S100a9* deficiency, paquinimod had no impact on Eotaxin, IL-5, IL-9, IL-13, IL-17, MMP-2, MMP-8, MMP-12, p38, JNK, and c-Src (Supplemental Fig. S5 (https://figshare.com/s/cb18e8b7c6ac5dd6ff86)). Therefore, paquinimod treatment mimics the profile of *S100a9* deficiency, by modulating kinase, cytokine, and protease responses.

Paquinimod treatment slows the progression of already established smoke-induced COPD and age-related in mice. To confirm that paquinimod could be used to treat already established COPD, paquinimod was administered to mice following 2-months of cigarette smoke exposure. The animals were exposed for an additional 2 months with daily paquinimod intervention (Fig. 7).

Similar to the *S100a9*$^{-/-}$ mouse and early treatment with paquinimod, delayed paquinimod treatment prevented smoke-induced ERK and c-RAF phosphorylation (Fig. 7A), loss of lung function, airspace enlargements and tissue destruction (Fig. 7B-C), immune cell infiltration (Fig. 7D), MCP1, IL6 and KC (Fig. 7E) and MMP-3, MMP-9 and desmosine release (Fig. 7F). Therefore, paquinimod treatment successfully attenuated several key factors associated with COPD progression.

Lung function declines with advancing age (60) and S100A9 levels increase with age (68). Therefore, we examined whether administering paquinimod to aged animals could influence of lung function in the absence of cigarette smoke exposures. Paquinimod was administered to 18-month-old mice for 2-months (Fig. 8). Treatment reduced loss of lung function, airspace enlargements (Fig. 8A-B), IL6, KC, and MMP-3 release (Fig. 8C). Therefore, age-dependent S100A9 signaling contributes to loss of lung function and can be modulated by treatment with paquinimod.

ERK/c-RAF regulates S100A9-mediated cytokine and protease responses in human pulmonary fibroblasts. We previously demonstrated that S100A9 protein induces TLR4 signaling, ERK phosphorylation, secretion of MCP1 and IL8 in human primary small airway epithelial cells (24). However, to investigate MMP-3 changes we utilized human primary fibroblasts as they appear to be the only pulmonary cells expressing MMP-3 when utilizing the single-cell sequencing tool outlined by Reyfman *et al* (52). We treated fibroblasts with ERK (LY3214996) and c-RAF (GW5074) inhibitors prior to S100A9 stimulation. Fibroblasts were

treated with combined concentrations that induced no cell death, determined by LDH release assays (Fig. 9A). Inhibition of ERK or c-RAF prevented S100A9 induction of MCP-1, IL6, IL8, MMP-3, and MMP-9 gene expression (Fig. 9A).

S100A9 promotes fibroblast growth and activation to secrete cytokines and collagen production, via RAGE, ERK, MAPK and NF-κB pathways (79). Therefore, we examine whether TLR4, RAGE (AGER) or EMMPRIN (BSG) were required to regulate S100A9-dependent ERK and c-RAF phosphorylation. Utilizing siRNA (Supplemental Fig. S6 (https://figshare.com/s/6c700ca1c3e055ee3aef)), we observed that S100A9 can induce ERK and c-RAF phosphorylation via all three receptors (Fig. 9B). Therefore, we cannot rule out any of these receptors in the regulation of ERK and c-RAF in S100A9-mediated signaling in fibroblasts.

Discussion

Here, we demonstrate that age and cigarette smoke exposure enhance lung levels of S100A9 and utilizing animal models of cigarette smoke-induced COPD, we confirm that S100A9 contributes to smoke-induced loss of lung function. Our findings demonstrate that targeting S100A9 signaling with an inhibitor, such as paquinimod, could slow the progression of cigarette smoke-associated COPD and age-associated loss of tissue function. Knock-out or inhibition of S100A9 attenuated loss of lung function, airspace enlargement, protease and cytokine release into the airways, elastin degradation and ERK/c-RAF phosphorylation. Changes in inflammation, kinase and protease responses could contribute to the protection of the lung to smoke inhalation in mice. Our data also confirms that

428 S100A9 triggers ERK and c-RAF phosphorylation through its receptors TLR4,
429 RAGE, and EMMPRIN. Equally, inhibition of ERK and c-RAF activity with
430 chemical inhibitors prevents S100A9-induced expression of MCP1, IL6, IL8,
431 MMP-3, and MMP-9 in pulmonary fibroblasts. There is a robust change in
432 S100A9 expression during aging, which coincided with changes in lung structure
433 and physiology. Since COPD is regarded as an age-related disease, targeting
434 S100A9 signaling may counter several elements of lung aging. Therefore, smoke
435 and age-related induction of S100A9 contributes to elevated kinases, protease
436 and cytokine responses that could collectively alter lung function (see Fig. 9C for
437 the proposed mechanism scheme).

438 S100A9 expression is associated with aging, particularly in the central
439 nervous system (68). Interestingly, C57BL/6 mice do not have changes in
440 S100A9 expression in their lungs due to aging (68). However, this was reported
441 to be strain-dependent as the same group showed significant age-dependent
442 changes in S100A9 expression in CB6F1 mice (68). Here we observe changes in
443 S100A9 expression in both C57BL/6J and A/J mice when comparing young and
444 old animals, both in lung expression and secretion into the airways. We also see
445 a correlation with age and S100A9 BALF concentration in human samples.
446 Elevated age-related S100A9 expression in mice is partially due to the E26
447 transformation-specific (ETS) transcription factor SPI1/PU.1 (68). PU.1 is
448 upregulated in fibroblasts of various fibrotic diseases and regulate fibrosis (76).
449 There is evidence to suggest that PU.1 plays a role in COPD, with increased
450 transcriptional activity in mice susceptible to cigarette smoke-induced COPD (9).
451 Interestingly, vitamin D receptor (VDR) deficient mice develop emphysema

452 possibly due to the interaction of the VDR with PU.1 (36). PU.1 can also
453 modulate T cell receptor expression levels in CD4+ T cells via regulating the
454 DNA-binding activity of GATA-3 and subsequentially regulating Th2 development
455 (12). PU.1 also helps macrophage maintain identity through controlling the miR-
456 424-dependent translational repression of the nuclear factor 1 A-type protein
457 (54). S100A9 expression is also sensitive to the Src kinase inhibitor PP2 (65) and
458 STAT3 expression (39). We have previously identified that protein tyrosine
459 phosphatase 1B (PTP1B) is a major negative regulator of S100A9 expression
460 (24). Long-term exposure to cigarette smoke desensitizes PTP1B, resulting in
461 persistent inflammatory signaling (24, 30) and exposing *Ptp1b*$^{-/-}$ mice to cigarette
462 smoke exaggerates immune cell infiltration in the BALF and increased air space
463 enlargement (24). The DEAD-box RNA helicase, DDX21, can also interact with
464 TRIF to mediate S100A9 signaling (70). Therefore, evidence suggests that
465 S100A9 and signaling that regulates its expression are altered due to aging or
466 exposure to cigarette smoke. S100A9 induces senescence in mesenchymal
467 stromal cells, which triggers inflammasome responses (63). Further studies are
468 required whether S100A9 is inducing senescence in COPD. It is also noteworthy
469 to highlight that there are posttranslational changes that occur to S100A9 that
470 could influence its responses. Relatively few proteins are targets of S-
471 nitrosylation but both S100A8 and S100A9 can undergo S-nitrosylation by nitric
472 oxide (NO) donors, which alters their immune modulation responses, including
473 leukocyte-endothelial cell interactions (41). Equally, the phosphorylated form of
474 S100A9 is a potent inducer of cytokines (59) but little is known about the impact
475 of cigarette smoke on S100A9 phosphorylation and subsequent binding to

476 S100A8. Finally, S100A9 directly interacts with S100A8 and forms hetero-
477 tetramers and dimers. Therefore, the relationship of S100A9 with S100A8 also
478 requires addressing in COPD.

479 S100A9 is highly expressed in early infiltrating phagocytes (2) but S100A9
480 also influences leukocyte recruitment (56). We observe strong staining for
481 S100A9 in immune cells within the lung but also positive staining in the
482 epithelium. Profiling S100A9 positive cells within the lung would be of interest.
483 Equally, examining the significance of neutrophil S100A9 in cell specific animal
484 models would further increase our knowledge of S100A9 in COPD. S100A9
485 stimulates the shedding of L-selectin, up-regulates and activates Mac-1/CD11b,
486 and induces neutrophil adhesion to fibrinogen (56). This is important in COPD, as
487 L-selectin plays a major role in leukocyte recruitment (31) and leukocytes are
488 elevated in COPD airways and their intracellular components, notably proteases,
489 modulate extracellular matrix remodeling (75). S100A8 increases protease
490 expression and activation *in vivo*, including MMP-2, -3, -9, -13, ADAMS -4 and -5
491 (71). However, little is known about S100A9 induction of proteases in the lungs.
492 S100A9 binds to EMMPRIN, an inducer of matrix metalloproteinase synthesis, to
493 regulate MMP1 expression in a melanoma cell model (34). In human
494 osteoarthritis synovium, paquinimod treatment blocked MMP-1 and MMP-3
495 secretion (58). Here we observed that MMP-3 and MMP-9 are sensitive to
496 S100A9 signaling during smoke exposure. MMP-1 is not expressed by mice but
497 could also be mediated by S100A9 as TLR4 regulates its expression (28). MMP-
498 9 is well documented to potentially play a role in COPD development (22).
499 However, less is known about MMP-3 in COPD. MMP3 polymorphisms are

associated with cancer development in COPD patients (8). We observed reduced desmosine in the BALF of *S100a9*$^{-/-}$ and paquinimod treated animals. Changes in MMP-9 levels could contribute to this but other proteases may also contribute to the degradation of elastin. S100 proteins also activates neutrophils (18) and S100A9 directly binds p67phox and p47phox (18) to potentate NADPH oxidase activation in neutrophils. Therefore, inhibition of S100A9 could also prevent neutrophil-associated inflammation in COPD lungs in addition to preventing immune cell recruitment, and expression of tissue-damaging cytokines and proteases.

S100A9 signaling is associated with multiple diseases but it has a high affinity for lung localization, as B16F10 melanoma cells preferentially metastasize to the lungs and overexpress S100A8 and S100A9 in uteroglobin knockout mice and S100A9 is expressed highest in the lungs of uteroglobin knockout mice and are sensitized to RAGE signaling (57). Importantly, we previously demonstrated that RSV-infected human bronchial epithelial (HBE) cells, isolated from COPD donors, and fully differentiated and cultured in air-liquid interface secreted more S100A9 into the apical surface compared to cells from nonsmokers (24). Equally, exposing HBE cells isolated from COPD donors to S100A9 protein resulted in greater G-CSF and MCP-1 secretion than cells from smokers and non-smokers (24). Equally, cigarette smoke extract causes nitric oxide (NO) synthesis changes with CSE causing an irreversible inhibition of eNOS activity observed in pulmonary artery endothelial cells (67). S100A9 also promotes inflammation via the activation of TLR4 (72), RAGE (33) and CD147/ EMMPRIN (46). Cigarette smoke is known to modulate signaling of TLR4 (28), RAGE (53) and EMMPRIN

524 (7). Therefore, not only does smoke increase S100A9 expression, but it also
525 enhances the responses of known S100A9 receptors. S100A9 mediates ERK
526 and c-Raf signaling that could influence many downstream responses, including
527 ribosomal S6 kinases (27), cell cycle proteins, and mRNA translation mediated
528 proteins (55). ERK1/2 is closely associated with cell aging due to its regulation of
529 proliferation, senescence and mitochondria fate (80). Uniquely here we observe
530 that S100A9 did not influence c-Src, p38 or JNK responses. Most stimuli that
531 activate p38 also activate JNK (38). We previously observed that smoke induced
532 c-Src via PKC-α responses (29), which appear to be independent of S100A9
533 despite ERK being sensitive to c-Src activity.

534 Paquinimod, the S100A9 inhibitor used in this study, effectively treats
535 experimental lupus and encephalomyelitis (32) and is well tolerated in patients
536 with systemic lupus erythematosus (5). Paquinimod can influence macrophage
537 populations (66), T cell proliferation (32) and prevent S100A9 from being a
538 chemoattractant (56). Paquinimod prevents S100A9 binding to these receptors
539 (73). Paquinimod also reduces activation of disease-promoting transgenic natural
540 killer T-II cells and CD115+ Ly6Chi monocytes and CD11b+ F4/80+ CD206+
541 macrophages, which coincided with reduced liver fibrosis in an animal model
542 (26). Our paquinimod data suggest that paquinimod may be a good candidate for
543 treating COPD and due to its role in fibrosis, and it could possibly be utilized in
544 pulmonary fibrosis (79). However, it should also be noted that the role of S100A9
545 in bacterial pathogen clearance needs to be investigated in the context of COPD
546 exacerbations. S100A9 is linked to disease severity in sepsis shock (1, 19),
547 effect on neutrophil recruitment in *Streptococcus pneumoniae* (51), and

Salmonella infection (17) without impacting the bacterial load. However, *S100a9*$^{-/-}$ mice infected intranasally with pneumococci rapidly have elevated mortality (16). Equally, S100A9 protects from CD4+ T-helper type 2 cell hyperinflammation in response to *Alternaria alternata* (47). Therefore, additional studies on paquinimod during infection are required. Finally, S100A8 was recently shown to protect type II pneumonocytes from smoke-induced cell death (42). Whether S100A9 plays a similar role is unknown, and despite both proteins frequently interacting, both proteins also have independent signaling. Further studies on the interactions of both proteins in COPD and intracellular S100A9 signaling are required. Therefore, S100A9 or the proteins it interacts with could have multiple roles in the lungs of COPD patients and requires further studies to observe any plausible complications from long-term inhibition of S100A9. Finally, the correlation analysis in our study for human S100A9 BALF levels and age were not altered for possible confounding factors such as race, BMI, FEV1, and DLCO. Whether these or other factors contribute to S100A9 levels need to be explored further.

Together, our data identify that cigarette smoke-induced S100A9 contributes to loss of lung function, airspace enlargements, elastin degradation, enhanced phosphorylation of ERK and c-RAF, and altered expression of MMP-3, MMP-9, MCP-1, IL-6, and KC/IL-8. Smoke and age-dependent modulation of this pathway contribute to cigarette smoke-induced COPD.

Acknowledgments

The authors would like to thank the Pulmonary Division of SUNY Downstate Medical Centre for their support. Paquinimod was provided by Active Biotech AB, Sweden.

Grants

This work was supported by grants made available to P.G. (Flight Attendant Medical Research Institute (YCSA113380 and CIA160005) and the Alpha-1 Foundation (493373 and 614218).

Disclosures

Authors declare that they have no conflict of interest.

References

1. **Alkhateeb T, Kumbhare A, Bah I, Youssef D, Yao ZQ, McCall CE, and El Gazzar M**. S100A9 maintains myeloid-derived suppressor cells in chronic sepsis by inducing miR-21 and miR-181b. *Mol Immunol* 112: 72-81, 2019.
2. **Averill MM, Kerkhoff C, and Bornfeldt KE**. S100A8 and S100A9 in cardiovascular biology and disease. *Arterioscler Thromb Vasc Biol* 32: 223-229, 2012.
3. **Bah I, Kumbhare A, Nguyen L, McCall CE, and El Gazzar M**. IL-10 induces an immune repressor pathway in sepsis by promoting S100A9 nuclear localization and MDSC development. *Cell Immunol* 332: 32-38, 2018.
4. **Barnes PJ**. Inflammatory mechanisms in patients with chronic obstructive pulmonary disease. *J Allergy Clin Immunol* 138: 16-27, 2016.
5. **Bengtsson AA, Sturfelt G, Lood C, Ronnblom L, van Vollenhoven RF, Axelsson B, Sparre B, Tuvesson H, Ohman MW, and Leanderson T**. Pharmacokinetics, tolerability, and preliminary efficacy of paquinimod (ABR-215757), a new quinoline-3-carboxamide derivative: studies in lupus-prone mice and a multicenter, randomized, double-blind, placebo-controlled, repeat-dose, dose-ranging study in patients with systemic lupus erythematosus. *Arthritis and rheumatism* 64: 1579-1588, 2012.
6. **Berthier S, Paclet MH, Lerouge S, Roux F, Vergnaud S, Coleman AW, and Morel F**. Changing the conformation state of cytochrome b558 initiates NADPH oxidase activation: MRP8/MRP14 regulation. *J Biol Chem* 278: 25499-25508, 2003.

7. **Betsuyaku T, Tanino M, Nagai K, Nasuhara Y, Nishimura M, and Senior RM**. Extracellular matrix metalloproteinase inducer is increased in smokers' bronchoalveolar lavage fluid. *Am J Respir Crit Care Med* 168: 222-227, 2003.

8. **Brzoska K, Bartlomiejczyk T, Sochanowicz B, Cymerman M, Grudny J, Kolakowski J, Kapka-Skrzypczak L, Kruszewski M, Sliwinski P, and Roszkowski-Sliz K**. Matrix metalloproteinase 3 polymorphisms as a potential marker of enhanced susceptibility to lung cancer in chronic obstructive pulmonary disease subjects. *Ann Agric Environ Med* 21: 546-551, 2014.

9. **Cabanski M, Fields B, Boue S, Boukharov N, DeLeon H, Dror N, Geertz M, Guedj E, Iskandar A, Kogel U, Merg C, Peck MJ, Poussin C, Schlage WK, Talikka M, Ivanov NV, Hoeng J, and Peitsch MC**. Transcriptional profiling and targeted proteomics reveals common molecular changes associated with cigarette smoke-induced lung emphysema development in five susceptible mouse strains. *Inflamm Res* 64: 471-486, 2015.

10. **Cazzola M, Page CP, Calzetta L, and Matera MG**. Emerging anti-inflammatory strategies for COPD. *Eur Respir J* 40: 724-741, 2012.

11. **Cesaro A, Anceriz N, Plante A, Page N, Tardif MR, and Tessier PA**. An inflammation loop orchestrated by S100A9 and calprotectin is critical for development of arthritis. *PLoS One* 7: e45478, 2012.

12. **Chang HC, Han L, Jabeen R, Carotta S, Nutt SL, and Kaplan MH**. PU.1 regulates TCR expression by modulating GATA-3 activity. *J Immunol* 183: 4887-4894, 2009.

13. **Choi IY, Gerlag DM, Herenius MJ, Thurlings RM, Wijbrandts CA, Foell D, Vogl T, Roth J, Tak PP, and Holzinger D**. MRP8/14 serum levels as a strong predictor of response to biological treatments in patients with rheumatoid arthritis. *Ann Rheum Dis* 74: 499-505, 2015.

14. **Cotoi OS, Duner P, Ko N, Hedblad B, Nilsson J, Bjorkbacka H, and Schiopu A**. Plasma S100A8/A9 correlates with blood neutrophil counts, traditional risk factors, and cardiovascular disease in middle-aged healthy individuals. *Arterioscler Thromb Vasc Biol* 34: 202-210, 2014.

15. **D'Armiento J, Dalal SS, Okada Y, Berg RA, and Chada K**. Collagenase expression in the lungs of transgenic mice causes pulmonary emphysema. *Cell* 71: 955-961, 1992.

16. **De Filippo K, Neill DR, Mathies M, Bangert M, McNeill E, Kadioglu A, and Hogg N**. A new protective role for S100A9 in regulation of neutrophil recruitment during invasive pneumococcal pneumonia. *FASEB J* 28: 3600-3608, 2014.

17. **De Jong HK, Achouiti A, Koh GC, Parry CM, Baker S, Faiz MA, van Dissel JT, Vollaard AM, van Leeuwen EM, Roelofs JJ, de Vos AF, Roth J, van der Poll T, Vogl T, and Wiersinga WJ**. Expression and function of S100A8/A9 (calprotectin) in human typhoid fever and the murine Salmonella model. *PLoS Negl Trop Dis* 9: e0003663, 2015.

18. **Doussiere J, Bouzidi F, and Vignais PV**. The S100A8/A9 protein as a partner for the cytosolic factors of NADPH oxidase activation in neutrophils. *Eur J Biochem* 269: 3246-3255, 2002.

19. **Dubois C, Marce D, Faivre V, Lukaszewicz AC, Junot C, Fenaille F, Simon S, Becher F, Morel N, and Payen D**. High plasma level of S100A8/S100A9 and

S100A12 at admission indicates a higher risk of death in septic shock patients. *Sci Rep* 9: 15660, 2019.

20. **Ehrchen JM, Sunderkotter C, Foell D, Vogl T, and Roth J**. The endogenous Toll-like receptor 4 agonist S100A8/S100A9 (calprotectin) as innate amplifier of infection, autoimmunity, and cancer. *J Leukoc Biol* 86: 557-566, 2009.

21. **Fischer BM, Pavlisko E, and Voynow JA**. Pathogenic triad in COPD: oxidative stress, protease-antiprotease imbalance, and inflammation. *Int J Chron Obstruct Pulmon Dis* 6: 413-421, 2011.

22. **Foronjy R, Nkyimbeng T, Wallace A, Thankachen J, Okada Y, Lemaitre V, and D'Armiento J**. Transgenic expression of matrix metalloproteinase-9 causes adult-onset emphysema in mice associated with the loss of alveolar elastin. *Am J Physiol Lung Cell Mol Physiol* 294: L1149-1157, 2008.

23. **Foronjy RF, Dabo AJ, Taggart CC, Weldon S, and Geraghty P**. Respiratory syncytial virus infections enhance cigarette smoke induced COPD in mice. *PLoS One* 9: e90567, 2014.

24. **Foronjy RF, Ochieng PO, Salathe MA, Dabo AJ, Eden E, Baumlin N, Cummins N, Barik S, Campos M, Thorp EB, and Geraghty P**. Protein tyrosine phosphatase 1B negatively regulates S100A9-mediated lung damage during respiratory syncytial virus exacerbations. *Mucosal Immunol* 2016.

25. **Foronjy RF, Taggart CC, Dabo AJ, Weldon S, Cummins N, and Geraghty P**. Type-I interferons induce lung protease responses following respiratory syncytial virus infection via RIG-I-like receptors. *Mucosal Immunol* 8: 161-175, 2015.

26. **Fransen Pettersson N, Deronic A, Nilsson J, Hannibal TD, Hansen L, Schmidt-Christensen A, Ivars F, and Holmberg D**. The immunomodulatory quinoline-3-carboxamide paquinimod reverses established fibrosis in a novel mouse model for liver fibrosis. *PLoS One* 13: e0203228, 2018.

27. **Frodin M, and Gammeltoft S**. Role and regulation of 90 kDa ribosomal S6 kinase (RSK) in signal transduction. *Mol Cell Endocrinol* 151: 65-77, 1999.

28. **Geraghty P, Dabo AJ, and D'Armiento J**. TLR4 protein contributes to cigarette smoke-induced matrix metalloproteinase-1 (MMP-1) expression in chronic obstructive pulmonary disease. *J Biol Chem* 286: 30211-30218, 2011.

29. **Geraghty P, Hardigan A, and Foronjy RF**. Cigarette smoke activates the proto-oncogene c-src to promote airway inflammation and lung tissue destruction. *Am J Respir Cell Mol Biol* 50: 559-570, 2014.

30. **Geraghty P, Hardigan AA, Wallace AM, Mirochnitchenko O, Thankachen J, Arellanos L, Thompson V, D'Armiento JM, and Foronjy RF**. The glutathione peroxidase 1-protein tyrosine phosphatase 1B-protein phosphatase 2A axis. A key determinant of airway inflammation and alveolar destruction. *Am J Respir Cell Mol Biol* 49: 721-730, 2013.

31. **Hafezi-Moghadam A, Thomas KL, Prorock AJ, Huo Y, and Ley K**. L-selectin shedding regulates leukocyte recruitment. *J Exp Med* 193: 863-872, 2001.

32. **Helmersson S, Sundstedt A, Deronic A, Leanderson T, and Ivars F**. Amelioration of experimental autoimmune encephalomyelitis by the quinoline-3-carboxamide paquinimod: reduced priming of proinflammatory effector CD4(+) T cells. *Am J Pathol* 182: 1671-1680, 2013.

33. **Hermani A, De Servi B, Medunjanin S, Tessier PA, and Mayer D**. S100A8 and S100A9 activate MAP kinase and NF-kappaB signaling pathways and trigger

translocation of RAGE in human prostate cancer cells. *Experimental cell research* 312: 184-197, 2006.

34. **Hibino T, Sakaguchi M, Miyamoto S, Yamamoto M, Motoyama A, Hosoi J, Shimokata T, Ito T, Tsuboi R, and Huh NH**. S100A9 is a novel ligand of EMMPRIN that promotes melanoma metastasis. *Cancer research* 73: 172-183, 2013.

35. **Hsia CCW, Hyde, D.M., Ochs, M., Weibel, E.R. and on behalf of the ATS/ERS Joint Task Force on the Quantitative Assessment of Lung Structure**. An Official Research Policy Statement of the American Thoracic Society/European Respiratory Society: Standards for Quantitative Assessment of Lung Structure. *Am J Respir Crit Care Med* 181: 394-418, 2010.

36. **Hu G, Dong T, Wang S, Jing H, and Chen J**. Vitamin D3-vitamin D receptor axis suppresses pulmonary emphysema by maintaining alveolar macrophage homeostasis and function. *EBioMedicine* 45: 563-577, 2019.

37. **Kim J, Bhattacharjee R, Snow AB, Capdevila OS, Kheirandish-Gozal L, and Gozal D**. Myeloid-related protein 8/14 levels in children with obstructive sleep apnoea. *Eur Respir J* 35: 843-850, 2010.

38. **Lee JC, Laydon JT, McDonnell PC, Gallagher TF, Kumar S, Green D, McNulty D, Blumenthal MJ, Heys JR, Landvatter SW, Strickler JE, McLaughlin MM, Siemens IR, Fisher SM, Livi GP, White JR, Adams JL, and Young PR**. A protein kinase involved in the regulation of inflammatory cytokine biosynthesis. *Nature* 372: 739-746, 1994.

39. **Li C, Zhang F, Lin M, and Liu J**. Induction of S100A9 gene expression by cytokine oncostatin M in breast cancer cells through the STAT3 signaling cascade. *Breast Cancer Res Treat* 87: 123-134, 2004.

40. **Lian Z, Wang L, Yamaga S, Bonds W, Beazer-Barclay Y, Kluger Y, Gerstein M, Newburger PE, Berliner N, and Weissman SM**. Genomic and proteomic analysis of the myeloid differentiation program. *Blood* 98: 513-524, 2001.

41. **Lim SY, Raftery M, Cai H, Hsu K, Yan WX, Hseih HL, Watts RN, Richardson D, Thomas S, Perry M, and Geczy CL**. S-nitrosylated S100A8: novel anti-inflammatory properties. *J Immunol* 181: 5627-5636, 2008.

42. **Lin CR, Bahmed K, Criner GJ, Marchetti N, Tuder RM, Kelsen S, Bolla S, Mandapati C, and Kosmider B**. S100A8 Protects Human Primary Alveolar Type II Cells against Injury and Emphysema. *Am J Respir Cell Mol Biol* 60: 299-307, 2019.

43. **Meyer KC**. The role of immunity and inflammation in lung senescence and susceptibility to infection in the elderly. *Semin Respir Crit Care Med* 31: 561-574, 2010.

44. **Miller MR**. Structural and physiological age-associated changes in aging lungs. *Semin Respir Crit Care Med* 31: 521-527, 2010.

45. **Ohnishi K, Takagi M, Kurokawa Y, Satomi S, and Konttinen YT**. Matrix metalloproteinase-mediated extracellular matrix protein degradation in human pulmonary emphysema. *Lab Invest* 78: 1077-1087, 1998.

46. **Olsson A, Nakhle J, Sundstedt A, Plas P, Bauchet AL, Pierron V, Bruetschy L, Deronic A, Torngren M, Liberg D, Schmidlin F, and Leanderson T**. Tasquinimod triggers an early change in the polarization of tumor associated macrophages in the tumor microenvironment. *J Immunother Cancer* 3: 53, 2015.

47. **Palmer LD, Maloney KN, Boyd KL, Goleniewska AK, Toki S, Maxwell CN, Chazin WJ, Peebles RS, Jr., Newcomb DC, and Skaar EP**. The Innate Immune

Protein S100A9 Protects from T-Helper Cell Type 2-mediated Allergic Airway Inflammation. *Am J Respir Cell Mol Biol* 61: 459-468, 2019.

48. **Petrache I, Natarajan V, Zhen L, Medler TR, Richter AT, Cho C, Hubbard WC, Berdyshev EV, and Tuder RM**. Ceramide upregulation causes pulmonary cell apoptosis and emphysema-like disease in mice. *Nat Med* 11: 491-498, 2005.

49. **Pouwels SD, Heijink IH, ten Hacken NH, Vandenabeele P, Krysko DV, Nawijn MC, and van Oosterhout AJ**. DAMPs activating innate and adaptive immune responses in COPD. *Mucosal Immunol* 7: 215-226, 2014.

50. **Pouwels SD, Nawijn MC, Bathoorn E, Riezebos-Brilman A, van Oosterhout AJ, Kerstjens HA, and Heijink IH**. Increased serum levels of LL37, HMGB1 and S100A9 during exacerbation in COPD patients. *The European respiratory journal* 2015.

51. **Raquil MA, Anceriz N, Rouleau P, and Tessier PA**. Blockade of antimicrobial proteins S100A8 and S100A9 inhibits phagocyte migration to the alveoli in streptococcal pneumonia. *J Immunol* 180: 3366-3374, 2008.

52. **Reyfman PA, Walter JM, Joshi N, Anekalla KR, McQuattie-Pimentel AC, Chiu S, Fernandez R, Akbarpour M, Chen CI, Ren Z, Verma R, Abdala-Valencia H, Nam K, Chi M, Han S, Gonzalez-Gonzalez FJ, Soberanes S, Watanabe S, Williams KJN, Flozak AS, Nicholson TT, Morgan VK, Winter DR, Hinchcliff M, Hrusch CL, Guzy RD, Bonham CA, Sperling AI, Bag R, Hamanaka RB, Mutlu GM, Yeldandi AV, Marshall SA, Shilatifard A, Amaral LAN, Perlman H, Sznajder JI, Argento AC, Gillespie CT, Dematte J, Jain M, Singer BD, Ridge KM, Lam AP, Bharat A, Bhorade SM, Gottardi CJ, Budinger GRS, and Misharin AV**. Single-Cell Transcriptomic Analysis of Human Lung Provides Insights into the Pathobiology of Pulmonary Fibrosis. *Am J Respir Crit Care Med* 199: 1517-1536, 2019.

53. **Robinson AB, Stogsdill JA, Lewis JB, Wood TT, and Reynolds PR**. RAGE and tobacco smoke: insights into modeling chronic obstructive pulmonary disease. *Front Physiol* 3: 301, 2012.

54. **Rosa A, Ballarino M, Sorrentino A, Sthandier O, De Angelis FG, Marchioni M, Masella B, Guarini A, Fatica A, Peschle C, and Bozzoni I**. The interplay between the master transcription factor PU.1 and miR-424 regulates human monocyte/macrophage differentiation. *Proc Natl Acad Sci U S A* 104: 19849-19854, 2007.

55. **Roux PP, and Blenis J**. ERK and p38 MAPK-activated protein kinases: a family of protein kinases with diverse biological functions. *Microbiol Mol Biol Rev* 68: 320-344, 2004.

56. **Ryckman C, Vandal K, Rouleau P, Talbot M, and Tessier PA**. Proinflammatory activities of S100: proteins S100A8, S100A9, and S100A8/A9 induce neutrophil chemotaxis and adhesion. *J Immunol* 170: 3233-3242, 2003.

57. **Saha A, Lee YC, Zhang Z, Chandra G, Su SB, and Mukherjee AB**. Lack of an endogenous anti-inflammatory protein in mice enhances colonization of B16F10 melanoma cells in the lungs. *J Biol Chem* 285: 10822-10831, 2010.

58. **Schelbergen RF, Geven EJ, van den Bosch MH, Eriksson H, Leanderson T, Vogl T, Roth J, van de Loo FA, Koenders MI, van der Kraan PM, van den Berg WB, Blom AB, and van Lent PL**. Prophylactic treatment with S100A9 inhibitor paquinimod reduces pathology in experimental collagenase-induced osteoarthritis. *Ann Rheum Dis* 74: 2254-2258, 2015.

59. **Schenten V, Plancon S, Jung N, Hann J, Bueb JL, Brechard S, Tschirhart EJ, and Tolle F**. Secretion of the Phosphorylated Form of S100A9 from Neutrophils Is Essential for the Proinflammatory Functions of Extracellular S100A8/A9. *Front Immunol* 9: 447, 2018.
60. **Schulte H, Muhlfeld C, and Brandenberger C**. Age-Related Structural and Functional Changes in the Mouse Lung. *Front Physiol* 10: 1466, 2019.
61. **Services USDoHaH**. The Health Consequences of Smoking—50 Years of Progress: A Report of the Surgeon General Atlanta: U.S. Department of Health and Human Services, Centers for Disease Control and Prevention, National Center for Chronic Disease Prevention and Health Promotion, Office on Smoking and Health: 2014.
62. **Shalaby KH, Gold LG, Schuessler TF, Martin JG, and Robichaud A**. Combined forced oscillation and forced expiration measurements in mice for the assessment of airway hyperresponsiveness. *Respir Res* 11: 82, 2010.
63. **Shi L, Zhao Y, Fei C, Guo J, Jia Y, Wu D, Wu L, and Chang C**. Cellular senescence induced by S100A9 in mesenchymal stromal cells through NLRP3 inflammasome activation. *Aging (Albany NY)* 11: 9626-9642, 2019.
64. **Simard JC, Girard D, and Tessier PA**. Induction of neutrophil degranulation by S100A9 via a MAPK-dependent mechanism. *J Leukoc Biol* 87: 905-914, 2010.
65. **Spijkers-Hagelstein JA, Schneider P, Hulleman E, de Boer J, Williams O, Pieters R, and Stam RW**. Elevated S100A8/S100A9 expression causes glucocorticoid resistance in MLL-rearranged infant acute lymphoblastic leukemia. *Leukemia* 26: 1255-1265, 2012.
66. **Stenstrom M, Nyhlen HC, Torngren M, Liberg D, Sparre B, Tuvesson H, Eriksson H, and Leanderson T**. Paquinimod reduces skin fibrosis in tight skin 1 mice, an experimental model of systemic sclerosis. *J Dermatol Sci* 83: 52-59, 2016.
67. **Su Y, Han W, Giraldo C, De Li Y, and Block ER**. Effect of cigarette smoke extract on nitric oxide synthase in pulmonary artery endothelial cells. *Am J Respir Cell Mol Biol* 19: 819-825, 1998.
68. **Swindell WR, Johnston A, Xing X, Little A, Robichaud P, Voorhees JJ, Fisher G, and Gudjonsson JE**. Robust shifts in S100a9 expression with aging: a novel mechanism for chronic inflammation. *Sci Rep* 3: 1215, 2013.
69. **Togo S, Holz O, Liu X, Sugiura H, Kamio K, Wang X, Kawasaki S, Ahn Y, Fredriksson K, Skold CM, Mueller KC, Branscheid D, Welker L, Watz H, Magnussen H, and Rennard SI**. Lung fibroblast repair functions in patients with chronic obstructive pulmonary disease are altered by multiple mechanisms. *Am J Respir Crit Care Med* 178: 248-260, 2008.
70. **Tsai SY, Segovia JA, Chang TH, Morris IR, Berton MT, Tessier PA, Tardif MR, Cesaro A, and Bose S**. DAMP molecule S100A9 acts as a molecular pattern to enhance inflammation during influenza A virus infection: role of DDX21-TRIF-TLR4-MyD88 pathway. *PLoS Pathog* 10: e1003848, 2014.
71. **van Lent PL, Grevers LC, Blom AB, Arntz OJ, van de Loo FA, van der Kraan P, Abdollahi-Roodsaz S, Srikrishna G, Freeze H, Sloetjes A, Nacken W, Vogl T, Roth J, and van den Berg WB**. Stimulation of chondrocyte-mediated cartilage destruction by S100A8 in experimental murine arthritis. *Arthritis and rheumatism* 58: 3776-3787, 2008.

72. **Vogl T, Tenbrock K, Ludwig S, Leukert N, Ehrhardt C, van Zoelen MA, Nacken W, Foell D, van der Poll T, Sorg C, and Roth J**. Mrp8 and Mrp14 are endogenous activators of Toll-like receptor 4, promoting lethal, endotoxin-induced shock. *Nat Med* 13: 1042-1049, 2007.
73. **Wache C, Klein M, Ostergaard C, Angele B, Hacker H, Pfister HW, Pruenster M, Sperandio M, Leanderson T, Roth J, Vogl T, and Koedel U**. Myeloid-related protein 14 promotes inflammation and injury in meningitis. *The Journal of infectious diseases* 212: 247-257, 2015.
74. **Wang S, Song R, Wang Z, Jing Z, Wang S, and Ma J**. S100A8/A9 in Inflammation. *Front Immunol* 9: 1298, 2018.
75. **Wight TN, Frevert CW, Debley JS, Reeves SR, Parks WC, and Ziegler SF**. Interplay of extracellular matrix and leukocytes in lung inflammation. *Cell Immunol* 312: 1-14, 2017.
76. **Wohlfahrt T, Rauber S, Uebe S, Luber M, Soare A, Ekici A, Weber S, Matei AE, Chen CW, Maier C, Karouzakis E, Kiener HP, Pachera E, Dees C, Beyer C, Daniel C, Gelse K, Kremer AE, Naschberger E, Sturzl M, Butter F, Sticherling M, Finotto S, Kreuter A, Kaplan MH, Jungel A, Gay S, Nutt SL, Boykin DW, Poon GMK, Distler O, Schett G, Distler JHW, and Ramming A**. PU.1 controls fibroblast polarization and tissue fibrosis. *Nature* 566: 344-349, 2019.
77. **Xiao R, Goldklang MP, and D'Armiento JM**. Parenchymal Airspace Profiling: Sensitive Quantification and Characterization of Lung Structure Evaluating Parenchymal Destruction. *Am J Respir Cell Mol Biol* 55: 708-715, 2016.
78. **Xie M, Liu X, Cao X, Guo M, and Li X**. Trends in prevalence and incidence of chronic respiratory diseases from 1990 to 2017. *Respir Res* 21: 49, 2020.
79. **Xu X, Chen H, Zhu X, Ma Y, Liu Q, Xue Y, Chu H, Wu W, Wang J, and Zou H**. S100A9 promotes human lung fibroblast cells activation through receptor for advanced glycation end-product-mediated extracellular-regulated kinase 1/2, mitogen-activated protein-kinase and nuclear factor-kappaB-dependent pathways. *Clin Exp Immunol* 173: 523-535, 2013.
80. **Zou J, Lei T, Guo P, Yu J, Xu Q, Luo Y, Ke R, and Huang D**. Mechanisms shaping the role of ERK1/2 in cellular senescence (Review). *Mol Med Rep* 19: 759-770, 2019.

Figure legends

Figure 1. Lung levels of S100A9 increase with aging and disease status in humans. (A) Human BALF S100A9 levels were quantified in BALF from nonsmokers, smokers, and COPD subjects. S100A9 levels were corrected to total BALF urea concentrations. (B) S100A9 levels were plotted against subject age for nonsmokers,

878 smokers and COPD. Graphs are represented as mean ± SD, where n≥11 per group. P
879 values shown when comparing both treatments connected by a line, were determined by
880 Mann Whitney tests. Linear regression and Pearson correlation coefficient were also
881 performed.

882

883 **Figure 2. Lung levels of S100A9 increase with aging and smoke exposure in mice.**
884 (A) S100A9 gene expression and BALF concentration was measured in young (7-weeks
885 old) and old (18-months old) C57BL/6J. (B) Negative pressure-driven forced expiratory
886 and forced oscillation technique maneuvers were performed in young and old animals.
887 Forced expiration extension (FEV) in the first 0.05 seconds of forced vital capacity
888 (FVC), compliance and pressure-volume loops with the area under the curve analysis
889 were determined in each animal. Mean linear intercepts (MLI) were measured in the
890 lungs of the mice to assess air space size and comparative histology images of the four
891 mouse groups are presented here (scale bars=500 μm). (C) IL-6 and KC levels were
892 quantified in BALF from young and old animals. (D) S100A9 gene expression and BALF
893 concentration was measured in 8-months old C57BL/6J following exposure to no smoke
894 (NS), 1-month (acute) or 6 months (chronic) of cigarette smoke. Graphs are represented
895 as mean ± S.E.M, where n≥4 per group. P values shown when comparing both
896 treatments connected by a line, were determined by Student's t-tests. (E) IHC was
897 performed for S100A9 (brown stain) in NS and chronic smoke exposed animals. IgG
898 negative control is also shown (scale bars=50 μm).

899

900 **Figure 3. *S100a9*$^{-/-}$ mice have reduced disease characteristics in a smoke exposure**
901 **model.** Wild type and *S100a9*$^{-/-}$ mice were exposed to smoke exposure daily for 6
902 months. (A-B) Negative pressure-driven forced expiratory and forced oscillation

technique maneuvers were performed in all animal groups. Forced expiration extension (FEV) in the first 0.05 seconds of forced vital capacity (FVC), compliance and pressure-volume loops with the area under the curve analysis were determined in each animal. (C) Mean linear intercepts (MLI) were measured in the lungs of the mice to assess air space size and comparative histology images of the four mouse groups are presented here (scale bars=200 μm). (D) Alveolar count and ductal/destructive fractions were quantified in each animal by parenchymal airspace profiling. Each measurement is the mean ± SEM. P values shown when comparing both treatments connected by a line, were determined by 2-way ANOVA with Tukey's post hoc test.

Figure 4. *S100a9* deficiency reduced inflammation and protease responses during smoke exposure. (A) BALF cellularity levels were examined in wild type and *S100a9*$^{-/-}$ animals after 6 months of smoke exposure. BALF concentrations for (B) MCP-1, IL-6, KC, (C) MMP-3, MMP-9, and desmosine were quantified using Luminex bead assays. (D) ERK and c-Raf phosphorylation were examined in lung tissue in smoke-exposed animals by Western blot and densitometry analysis. Graphs are represented as mean ± S.E.M, where n≥3 per group P values shown when comparing both treatments connected by a line, were determined by 2-way ANOVA with Tukey's post hoc test.

Figure 5. Administration of the S100A9 inhibitor paquinimod shows no toxicity in mice and prevents the development of smoke-induced COPD. A/J mice received paquinimod orally each day prior to smoke exposure. (A) At the end of the study liver to body weight ratios were determined. (B) Animal body weight was calculated throughout the study. FEV in the first 0.05 seconds of FVC, compliance and (C) pressure-volume loops with the area under the curve analysis were determined in each animal. (D) MLI

was measured in the lungs of the mice to assess air space size and comparative histology images of the four mouse groups are presented here (scale bars=500 μm). (E) Alveolar count and ductal/destructive fractions were quantified in each animal by parenchymal airspace profiling. Each measurement is the mean ± SEM. P values shown when comparing both treatments connected by a line, were determined by 2-way ANOVA with Tukey's post hoc test. Graphs with 2 groups were analyzed by Student's t-tests.

Figure 6. Paquinimod prevents inflammation and protease responses during smoke exposure. (A) BALF cellularity levels were examined in A/J animals when paquinimod was administered daily prior to daily smoke exposure. BALF concentrations for (B) MCP-1, IL-6, KC, (C) MMP-3, MMP-9, desmosine were quantified using Luminex bead assays. (D) ERK and c-Raf phosphorylation were examined in lung tissue in smoke-exposed animals by Western blot and densitometry analysis. Each well represents a different animal. Graphs are represented as mean ± S.E.M, where n≥5 per group. P values shown when comparing both treatments connected by a line, were determined by 2-way ANOVA with Tukey's post hoc test. Graphs with 2 groups were analyzed by Student's t-tests.

Figure 7. Delayed administration of paquinimod reduces the loss of lung function in smoke-exposed mice. (A) A/J mice were smoke-exposed for 4 months and began receiving paquinimod orally each day at the 2-month mark after initiation of smoke exposure. ERK and c-Raf phosphorylation were examined in lung tissue in smoke-exposed animals by Western blot and densitometry analysis. (B) FEV in the first 0.05 seconds of FVC, compliance and pressure-volume loops with the area under the curve

analysis were determined in each animal. (C) MLI was measured in the lungs of the mice to assess air space size and comparative histology images of the four mouse groups are presented here (scale bars=500 μm). Alveolar count and ductal/destructive fractions were quantified in each animal by parenchymal airspace profiling. (D) BALF cellularity levels were examined in A/J animals when paquinimod was administered daily prior to daily smoke exposure. BALF concentrations for (E) MCP-1, IL-6, KC, (F) MMP-3, MMP-9, and desmosine were quantified using Luminex bead assays. Graphs are represented as mean ± S.E.M, where n≥5 per group. P values shown when comparing both treatments connected by a line, were determined by 2-way ANOVA with Tukey's post hoc test. Graphs with 2 groups were analyzed by Student's t-tests.

Figure 8. Paquinimod reduces the loss of lung function in aged mice. 18-month-old C57BL/6J mice were administered paquinimod or vehicle orally each day for 2-months. (A) Pressure-volume loops with the area under the curve, FEV in the first 0.05 seconds of FVC, compliance analysis was determined in each animal. MLI was measured in the lungs of the mice to assess air space size and comparative histology images of the four mouse groups are presented here (scale bars=500 μm). (C) BALF concentrations for IL-6, KC, and MMP-3 were quantified using Luminex bead assays. Graphs are represented as mean ± S.E.M, where n=6 animals per group. P values shown when comparing both treatments connected by a line, were determined by Student t-tests.

Figure 9. ERK and c-RAF phosphorylation are required for S100A9 induction of cytokines and proteases in lung fibroblasts. (A) Fibroblasts from NS individuals were grown in media supplemented with the ERK inhibitor LY3214996 or the c-RAF inhibitor GW5074 and toxicity assays were performed, by measuring LDH release. Real-time

PCR analysis was performed on these cells to examine levels of MCP1-, IL-6, IL-8, MMP3, and MMP9. (B) Immunoblots subsequent densitometry analysis was performed in fibroblasts following silencing of TLR4, AGER, and BSG and ERK and c-RAF phosphorylation were determined. Data are represented as mean ± S.E.M., where each measurement was performed with n≥4 subjects per group. P values shown when comparing both treatments connected by a line, were determined by 2-way ANOVA with Bonferroni posttests or by Student's t-tests. (C) Possible signaling mechanism following age and cigarette smoke-induced S100A9 signaling.

Supplemental Material

Supplemental Figure 1: 10.6084/m9.figshare.12272816

Supplemental Figure 2: 10.6084/m9.figshare.12272858

Supplemental Figure 3: 10.6084/m9.figshare.12272864

Supplemental Figure 4: 10.6084/m9.figshare.12272876

Supplemental Figure 5: 10.6084/m9.figshare.12272888

Supplemental Figure 6: 10.6084/m9.figshare.12863831

Table 1. Patient demographics for BALF donors

	Non-Smoker	**Smoker**	**COPD**	**p-value**
Number	11	28	76	
Age (years)	57.6 ± 13.2	57.1 ± 8.9	61.1 ± 9.3	0.331
Gender (Male/Female)	6/5	15/13	42/34	0.483

Race (Caucasian/ Hispanic/African-American)	46.6%/46.6%/6.6%	25%/61%/14%	5.3%/92%/2.7%	0.154
Pack years	0 ± 0	30.2. ± 11.4	48.9 ± 3.1	>0.001
FEV1 % Predicted	102.1 ± 14.9	93.9 ± 10.3	59.9 ± 11.9	0.011
FVC % Predicted	96.9 ± 10.5	95.2 ± 11.7	81.8 ± 1.8	0.015
FEV1/FVC %	81.2 ± 6.7	80.6 ± 4.7	52.9 ± 6.4	>0.001
D_LCO % Predicted	102 ± 10.6	92.9 ± 10.8	69.5 ± 10.9	0.013

Figure 1

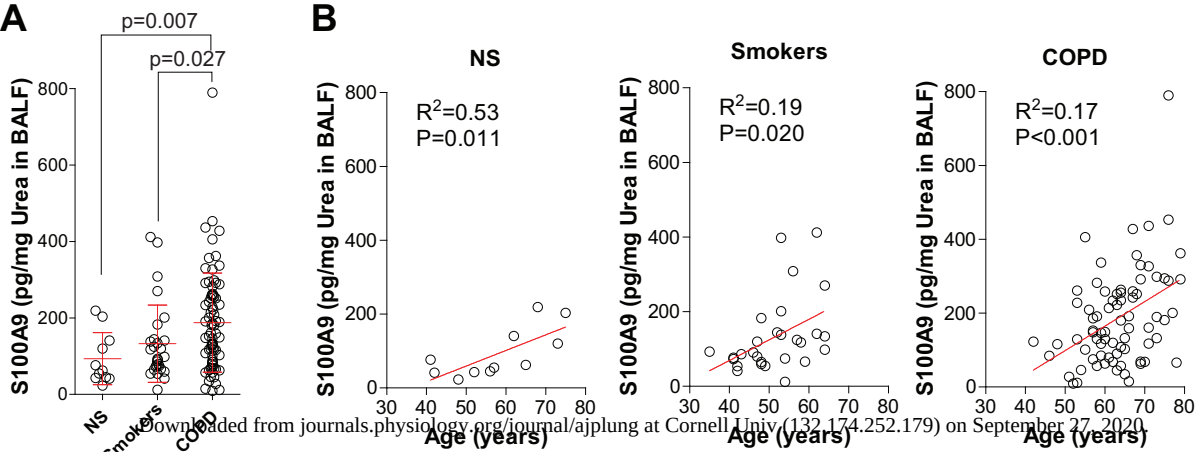

Figure 2

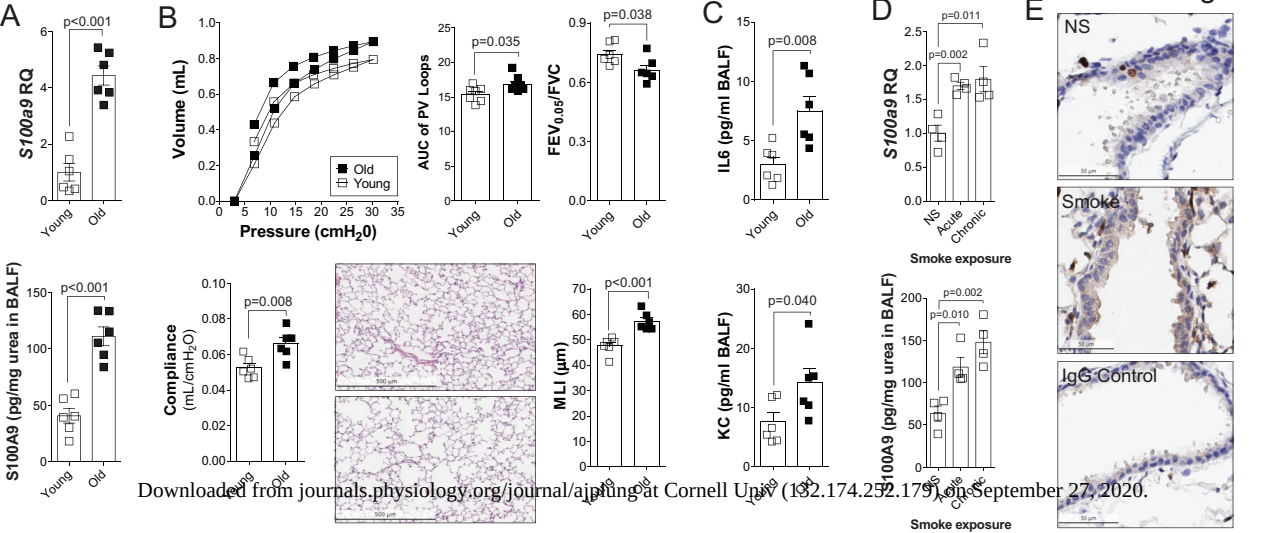

Figure 3

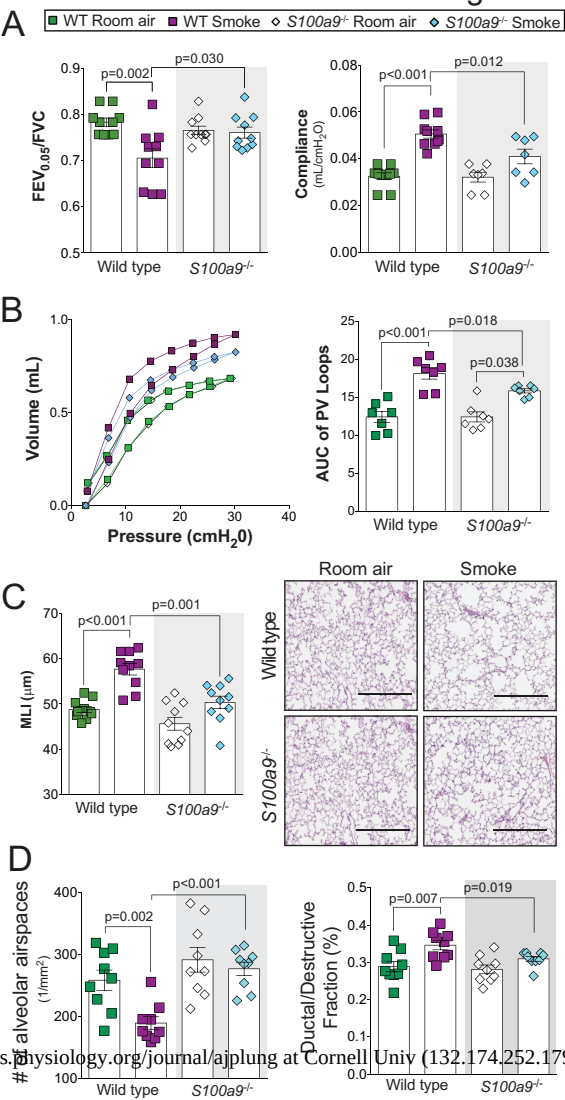

Figure 4

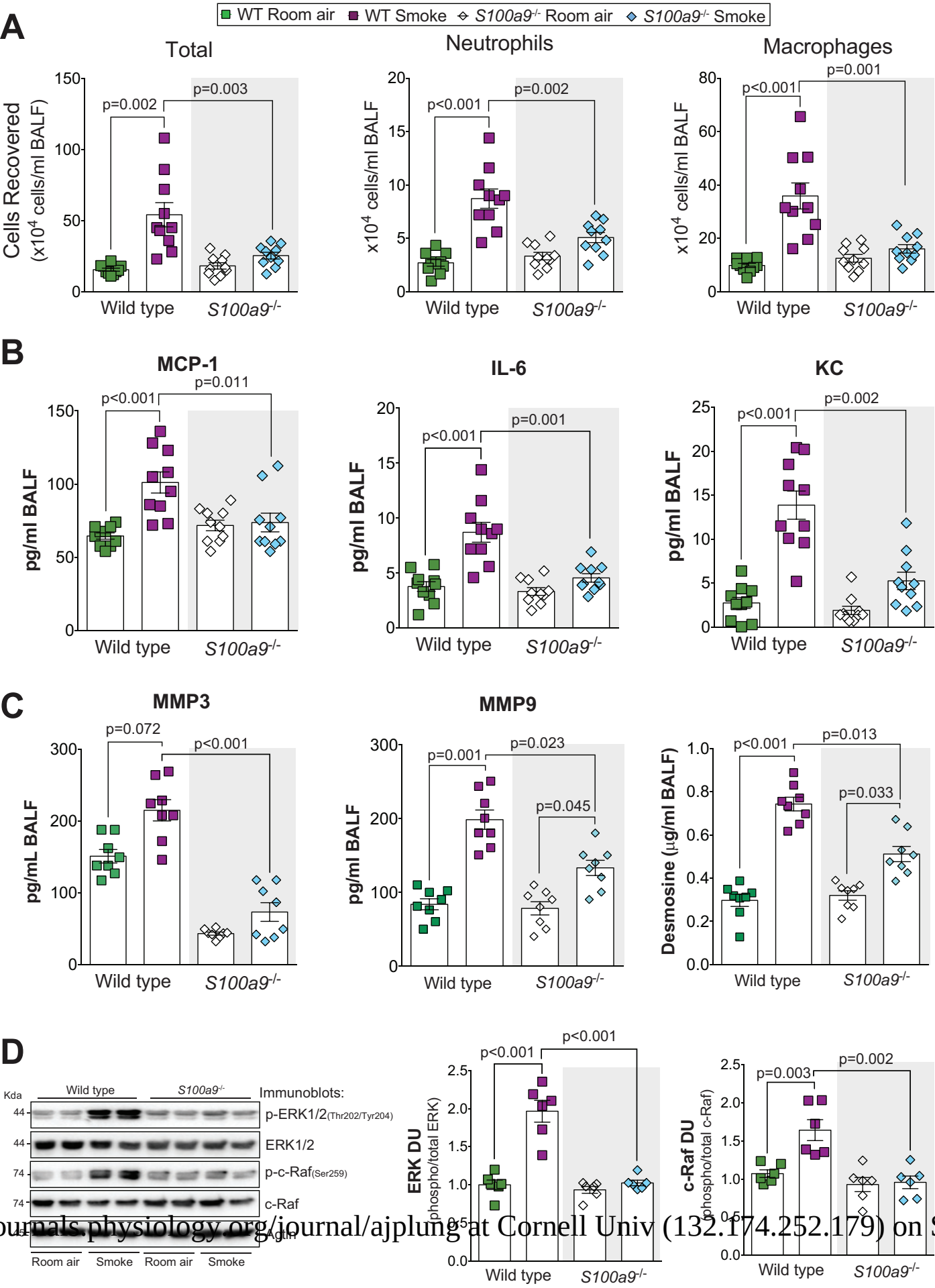

Figure 5

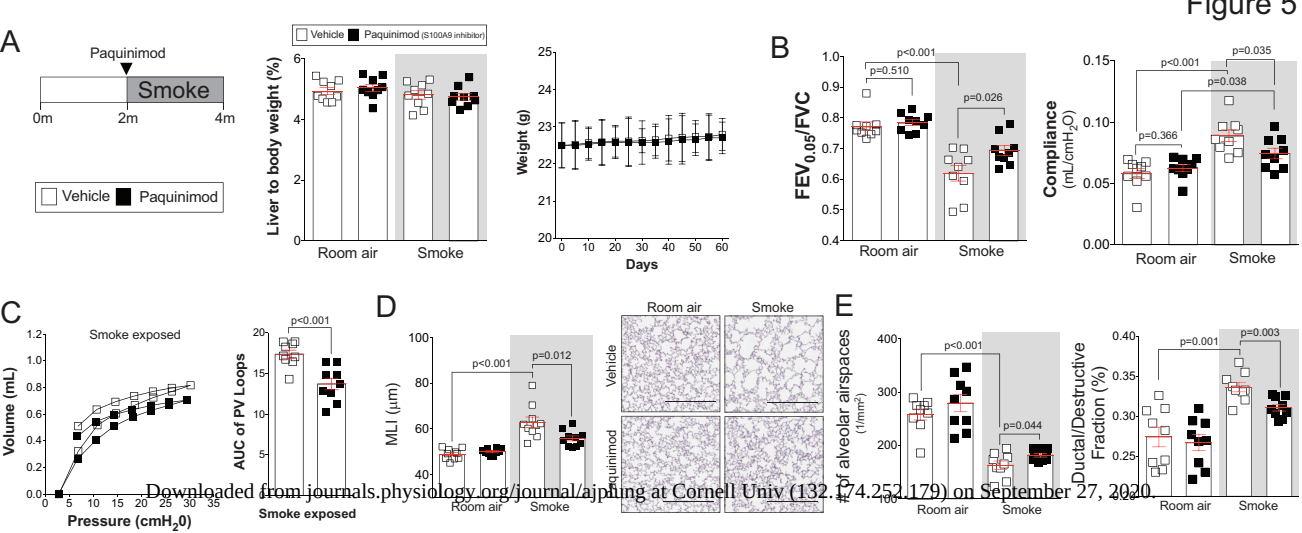

Figure 6

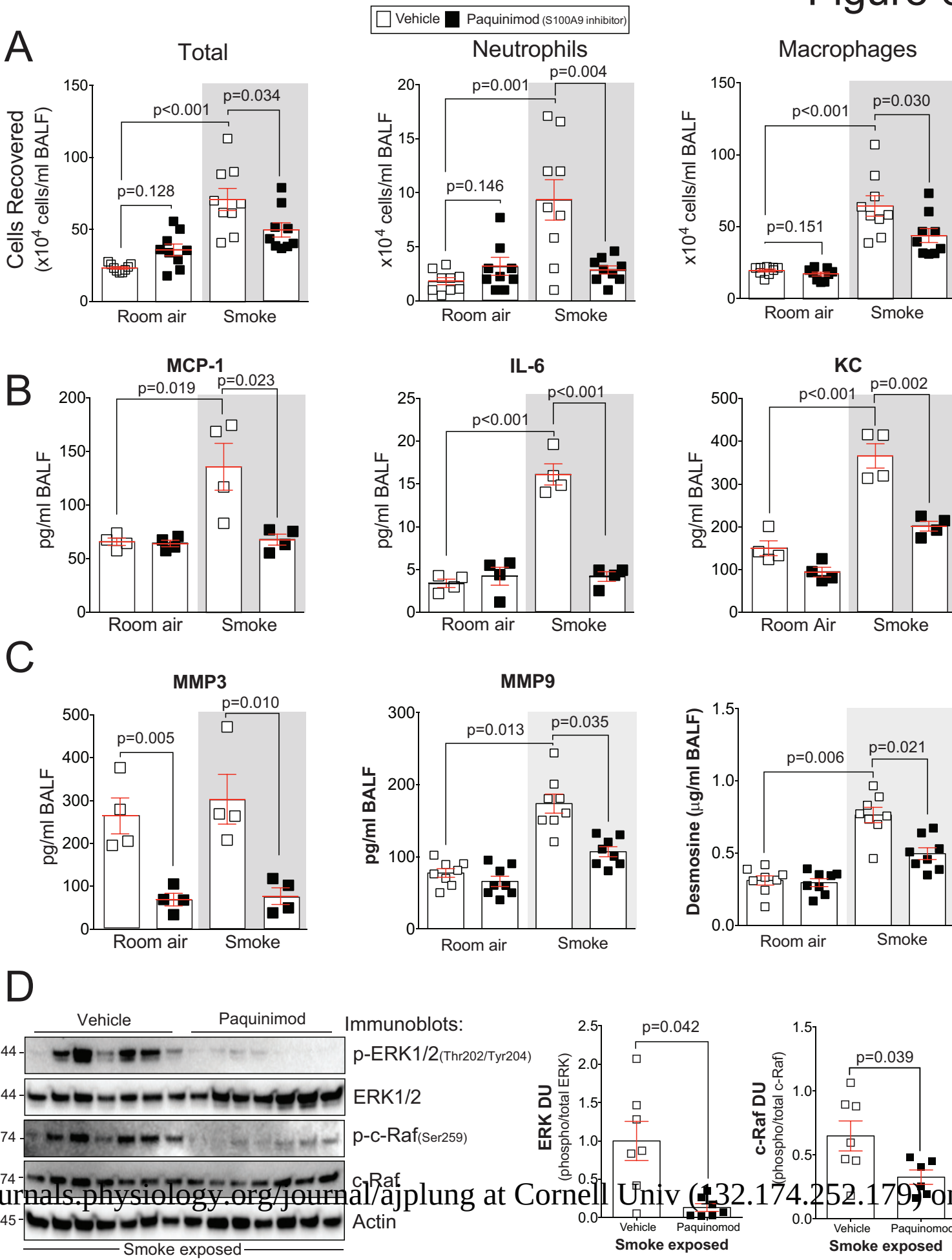

Figure 7

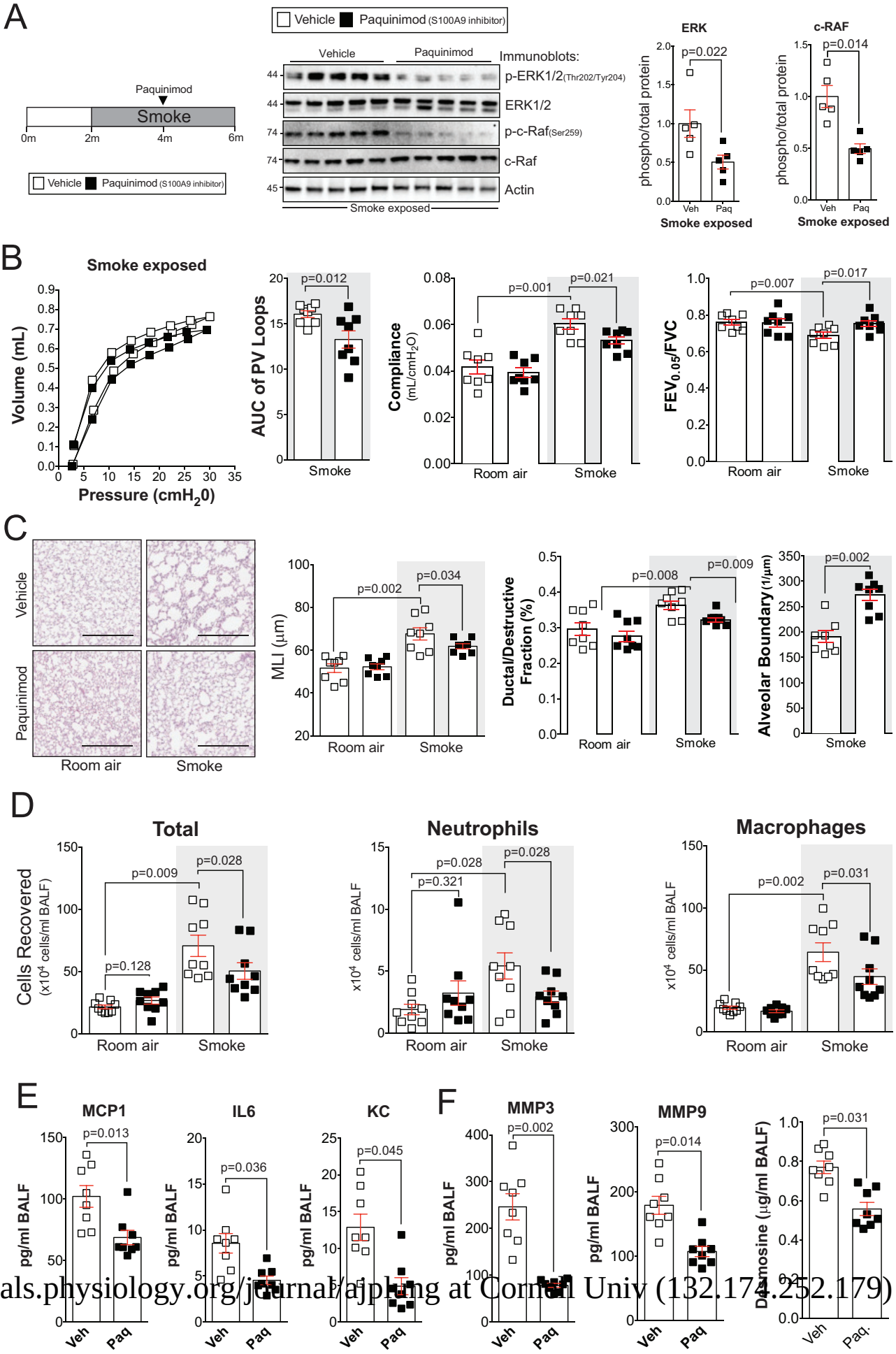

Figure 8

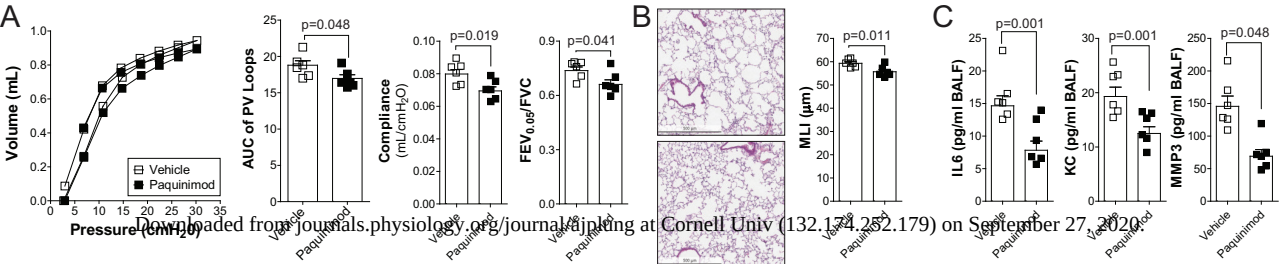

Figure 9